

Mechanical stimulation of primary cilia

Andrew Resnick¹, Ulrich Hoyer²

¹Department of Physiology and Biophysics, Case Western Reserve School of Medicine, 10900 Euclid Avenue, Cleveland OH 44106, ²Department of Physiology and Biophysics, Case Western Reserve School of Medicine, 10900 Euclid Avenue, Cleveland OH 44106

TABLE OF CONTENTS

1. Abstract
2. Introduction
3. Flow through ducts
 - 3.1. Coordinate system
 - 3.2. Poiseuille flow
 - 3.3. Limitations of model
 - 3.4. Effect of projections
 - 3.5. Evaluation of 'k'
 - 3.6. Further developments
4. In vitro approximation for $U(r)$
 - 4.1. Flow chamber
 - 4.2. Body forces
 - 4.3. Optical tweezer
 - 4.3.1. Principles of operation
 - 4.3.2. Biological considerations
 - 4.3.3. Trap strength measurement
 - 4.4. Summary
5. Bending of a cilium
6. Perspective
7. Biological effects
 - 7.1. Cellular level
 - 7.2. Organ level
 - 7.3. Organism level
8. Defining experiments
9. Conclusion
10. Acknowledgement
11. References

1. ABSTRACT

The ciliary/flagellar system is perhaps unique in biology in that not only are biochemical manipulations used to elucidate the function, but physical manipulations as well. Thus, there is a considerable need to have an integrated physical-biochemical model of a cilium and its function. The emphasis of this paper will be to firstly, provide a mechanistic picture of the cilium and its environment because the biological community is perhaps less aware of this type of model development, and second, to point the way towards future experiments that will elucidate the role of the cilium in organ and organism level signaling and regulation.

2. INTRODUCTION

Just as there are 'mouse models' for disease and *in vitro* models for biochemical processes, and in as much as cell cultures are model systems to study physiological processes, mathematical models of real objects simplify and omit extraneous details. What is important when selecting a particular model is to retain some essential component of the problem of interest. In this spirit, the bulk of this paper will cover ductal flow over primary (nonmotile) cilia as this represents from a physical point of view the most simple relevant system while still retaining the essential ingredients. We will indicate along the way how this simple model can be extended to other systems,

Mechanical stimulation of primary cilia

primarily ducts containing a brush border, a dense array of microvilli projecting into the lumen, which occurs in the proximal tubule segment of a nephron, or ducts containing motile cilia. Specifically, we are concerned with renal tubules (proximal tubule, loop of Henle, and collecting duct), but our results are also relevant to other, similar, ductal systems.

Our hypothesis is simply this: fluid flow bends the cilium, converting kinetic energy of the fluid into elastic energy, which drives strain-sensitive proteins to initiate or participate in flow-dependant signaling and regulatory processes. It is important to note that this hypothesis has several testable predictions, some of which have already been confirmed by experiment. Some specific predictions of this hypothesis are that sensitivity to flow depends on ciliary length, the greatest strain energy due to bending of a cilium is located at its base, and the orientation of tensile and compressive strain in the cilium is determined by the direction of the fluid flow. Biological sequella of these predictions may be that ciliary length is regulated, that relevant strain-sensitive proteins will be localized to the base of the cilium, and that spatially directed cell division and growth can occur in proliferating epithelia.

We also note that ciliated ducts typically connect non-ciliated structures. In the kidney, a duct connects the glomerulus to the renal pelvis. In the digestive system, the biliary ducts connect the liver and duodenum. The pancreatic ducts connect the acinii to the small intestine. Thus, our hypothesis can also imply that sensory cilia are used to monitor total amounts of a secreted substance. That is, if the concentration of a solute and fluid flow rate are sensed and integrated by cells, the total amount of a substance secreted by an upstream structure can conceivably be calculated.

In order to prove or disprove our hypothesis, we require physical information about the fluid environment around a cilium and information about the mechanical response of the cilium to the fluid action. Additionally, we require information about biochemical processes initiated upon (physical) stimulation of the cilium. Some of this information can be generated *a priori* from established physical law, while the remainder requires data from physiological and genetic experiments. Consequently, we first derive some simple models for the *in vivo* mechanical environment of the cilium (section 3), next, *in vitro* approximations (section 4), and finally, we describe the effect mechanical forces have on the cilium.

We model the cilium as a cylindrical rod of radius 'a' capped by a hemisphere. As fluid with dynamic viscosity μ (or kinematic viscosity $\nu = \mu/\rho$) and velocity U moves past a cilium, a drag force develops which can bend the cilium. For a half-sphere of diameter '2a', this drag force (f) is simply $f = 3\pi\mu aU$. Calculating the drag force per unit length against a cylinder of diameter '2a' is considerably more complex, but was solved by Oseen (1) for low Reynolds number (see below for the meaning of this number) and given by:

Eq.1

$$f = \frac{4\pi\mu U}{\frac{1}{2} - \gamma - \ln\left[\frac{2aU}{8\nu}\right]} = \frac{4\pi\mu U}{2.002 - \ln[\text{Re}]},$$

where γ is Euler's constant (0.577...) and $\text{Re} = \text{Reynolds number}$, given as $\text{Re} = 2aU/\nu$. (An alternative equivalent formulation of Eq 1 is $f = \frac{4\pi\rho U^2 2a}{\text{Re}(2.002 - \ln[\text{Re}])}$ used by

Schwartz *et al*, (60).

The total drag force on a cilium is then given schematically by (2):

$$\text{Eq.} \quad 2 \quad F_{\text{total}} = \int_{\text{Tubule wall } (s=0)}^{\text{Cilium tip } (s=L)} \frac{4\pi\mu U(s)}{2.002 - \ln[\text{Re}(s)]} \cdot ds + 3\pi\mu aU(s=L),$$

Where 's' is the coordinate along the axoneme of the cilium and $L = \text{cilium height}$ (see Section 5 of this paper for more detail).

Thus, in order to calculate the force incident on a cilium and the response of a cilium to this force, we must first know the fluid velocity as a function of height along the cilium, which we calculate next.

3. FLOW THROUGH DUCTS

The central thesis is that the cilium is used by the cell to gain information about the fluid flow through a duct. Proof or disproof of this thesis requires information about the flow profile. We develop a mathematical description for slow flow through long cylindrical tubes which may contain protrusions (cilia, brush border) into the lumen. There are several ciliated ductal systems that could be described by this simple model: the renal ducts, the biliary ducts, pancreatic ducts, and the developing bronchi and oviducts. For all of these tubes, their length is much longer than their diameter, they have long straight sections and their diameter is nearly constant over a considerable length. Thus, we idealize a real tubule by an artificial tubule which is strictly uniform, straight, and perfectly rigid. Later, we will discuss modifications to the model to more accurately mirror a real tubule. We note in passing that the mature airway fails to meet any of the simple approximations we make here, and so falls outside of the scope of this manuscript.

3.1. Coordinate systems

The coordinate system for tube flow is defined in Figure 1.

We approximate the luminal space within a duct as an infinitely long uniform cylinder of radius 'R'. These geometrical assumptions simplify the mathematics. Failure to reconcile theory with experiment could be due to instability of the exact mathematical solution to small perturbations that can occur in real systems. This point will be revisited periodically throughout the paper.

Mechanical stimulation of primary cilia

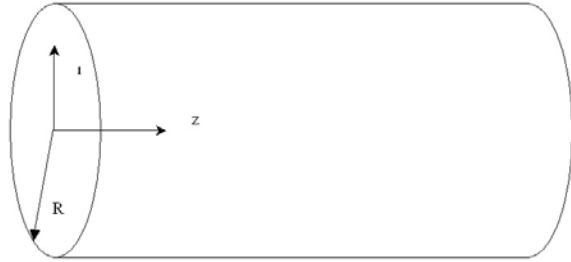


Figure 1. Coordinate systems for a cylindrical tubule with radius 'R'. The fluid flow is in the 'z' direction (axial). Ciliated cells are taken to lie at the outer perimeter of the cylinder ($r = R$) with the cilia growing along the 'r' axis. Thus, the axoneme of cilia are normal to the flow direction.

We first begin with a general mathematical model for fluid flow, because the fluid velocity gives us information about the physical environment of the cilium and how it is acted upon. We initially make no assumptions here about the type of fluid, how it is constrained, or how it moves. First consider Newton's second law generalized to a continuum, known as Cauchy's first law of motion:

$$\text{Eq. 3. } \rho \frac{DU}{Dt} = \nabla \cdot \mathbb{T} + F_b$$

Where ρ is the density of the medium, U the velocity, D/Dt

is the material derivative ($\frac{D}{Dt} = \frac{\partial}{\partial t} + U \cdot \nabla$), and \mathbb{T} the

stress tensor. We have implicitly set the density to be constant. F_b is called a 'body force' term and can be used to introduce gravity, centripetal force, friction, or a force applied from a motile cilium onto the fluid. The intuitive meaning of the material derivative can be explained

(fatuously) by the following device: $\frac{D[\text{the weather}]}{Dt}$

means the weather can change in two ways: either by sitting still and waiting ($\frac{\partial[\text{the weather}]}{\partial t}$) or by getting on

an airplane and going somewhere else ($U \cdot \nabla[\text{the weather}]$). For steady state conditions,

$\frac{\partial U}{\partial t} = 0$. The term $(U \cdot \nabla)U$ is nonlinear (U appears

twice) and for sufficiently slow flow (Reynolds number $\ll 1$), we can neglect this term.

For simple fluids (constant viscosity at a given temperature regardless of the rate of shear), the divergence of the stress tensor is given as

$$\text{Eq. 4. } \nabla \cdot \mathbb{T} = -\nabla P + \mu \nabla^2 U,$$

and Cauchy's first law is then referred to as the Navier-Stokes system of equations. For our geometries above, we are most interested in the axial component of flow for two reasons. First, the axial flow is likely to be much larger

than the radial flow. Second, the axial flow is perpendicular to the cilia and thus likely has a larger effect on the cilium. Consequently, we can again simplify the equations by assuming that the fluid velocity in the axial direction is a function only of the radial coordinate.

We have, as a beginning point, the steady-state Navier-Stokes equation for the axial (z) component of the fluid velocity U_z :

$$\text{Eq. 5. } 0 = -\frac{dP}{dz} + \mu \nabla^2 U_z + F_{b,z}$$

To completely solve any differential equation, either the function (Dirichlet boundary condition) or the derivative of the function (Neumann boundary condition) must be defined on a boundary. In fluid dynamics, perhaps the most important boundary condition is the no-slip condition. This boundary condition means that the velocity of a fluid layer adjacent to a solid surface is zero. This case gives rise to Poiseuille flow at low Reynolds numbers and will be discussed first and foremost. However, the no-slip condition does not hold for two relevant classes of biological problems- wetting (a solid surface partially covered by a moving fluid) and permeable boundaries. A simplified model that includes mass flow through the walls of the tube, corresponding to fluid and ion absorption will be presented below, while wetting is a subject beyond the scope of this manuscript.

3.2. Poiseuille flow

Because Poiseuille flow is covered in many other publications (3), we will only present the final results in Table 1. To simplify equations, the subscript 'z' in U_z will be dropped from now on when it is clear that only this component of U is discussed and the relevant flow qualities are expressed in terms of the volumetric flow rate

$$Q_v = 2\pi \int_0^R U(r) * r dr$$

rather than the pressure drop, as the former is more amenable to experimental manipulation and measurement. Note that the volumetric flow rate does not depend on fluid density, and is linearly proportional to the axial pressure gradient. The basic predictions of this model are the velocity profile $U(r)$ and maximum velocity U_{max} , which can be directly measured, and the wall shear stress and Reynolds number, which cannot.

The Reynolds number, in general, is defined as the ratio of inertial forces (kinetic energy) to viscous forces (dissipated energy) and mathematically expressed as $Re = \frac{lU}{\nu}$,

whereby l = a characteristic length constant and U and ν are as defined above (see also above the expression for the Reynolds number of a cylindrical projection). It has two important properties. On one hand, the Reynolds number contains information about the flow- whether the flow is laminar or turbulent. On the other hand, the Reynolds number also allows us to compare disparate systems (e.g. differently sized ducts, different fluid viscosities) in a rational manner.

Mechanical stimulation of primary cilia

Table 1. Characteristics of tube Poiseuille flow in terms of volumetric flow rate (Q_V)

| Geometry | Velocity profile $U(r)$ | Maximum velocity U_{max} | Reynolds Number Re |
|------------------|-----------------------------------|----------------------------|------------------------------|
| Cylindrical tube | $\frac{2Q_V}{\pi R^4}(R^2 - r^2)$ | $\frac{2Q_V}{\pi R^2}$ | $\frac{4\rho Q_V}{\pi\mu R}$ |

U = axial flow rate; R = tubule radius; r = radial distance from center of tube; ρ = fluid density; μ = fluid viscosity; Re = Reynolds number.

3.3. Limitations of model description

Conceptually, we made much use of things being ‘infinite’, ‘uniform’, concepts that are clearly unphysical. The important questions are what does this model predict, and which phenomena are currently unaccounted for? Because the simplified model here predicts results that are affirmed by experiment (for example, the volume of urine is proportional to proximal tubule pressure (4, 5) we argue that some essential physical features are already contained. However, there are fundamental processes within the renal tubule that are unaccounted for. Two examples are that fluid is resorbed through the walls of the proximal tubule (‘leaky tubules’), and another, that measurements have shown the pressure within renal tubules is subject to many external effects, including renal pelvic contractions (6). As to the first, we can incorporate permeable tube walls into the model (7-11). Although the details are beyond the scope of this paper, the result obtained using some well-justified simplifications (10) results in the volume flux as a function of position along the tubule wall to take the form $Q_V(z) = Q_V^0 e^{-\alpha z}$, where α is related to the permeability of the tubule wall and Q_V^0 is the volumetric flux at the tubule inlet. The volumetric flux decays exponentially along the length of the tubule.

Regarding the difficulty in quantitative description of the intratubule pressure, we can attempt to dispense with the problem also by working in terms of the volumetric flux. Although we do not include the explicit results here, the detailed solutions we obtain below still maintain a linear relationship between the pressure drop and volumetric flux. Consequently, when reconciling theory and experiment, one can simply measure the local volumetric flux and ignore the many processes which create a particular pressure drop.

Thus, both perturbations (leaky tubules, pelvic contractions) can be treated in a straightforward way by parameterizing the flow in terms of the local volumetric flow rate defined earlier.

Additionally, if one is interested comparing time-averaged versus acute stimulation of cilia, one may inquire as to the effects of pulsatile versus steady flow. In that case, one would allow the pressure to vary with time and then solve the time-dependent Navier-Stokes equations. Reasonable expressions can be obtained for simple time-dependent oscillations (12). Simple manipulations can include stepping type oscillations, square-wave type oscillations, having an oscillatory component in addition to a constant component- the goal being to capture essential components of pulsatile flow or to test the thesis of ultrafiltrate flow driven either by pelvic contractions or pulsatile circulation.

Micropuncture measurements of renal tubular flow generally present a maximum volumetric flow rate of

5 nl/min per nephron, and given a luminal radius of 10 microns, the Reynolds number for *in vivo* flow in a renal tubule can then be maximally estimated at 0.15. This indicates that we can safely omit the nonlinear term $(U \cdot \nabla)U$. Additionally, the turns and bends in the nephron do not produce a perturbation to the flow pattern, justifying our simplification of a straight tubule.

3.4. Effect of projections into lumen

When considering the effect of cilia or brush border on flow, there are two possible approaches. On one hand, one can assume the projections do not perturb the velocity profile and simply calculate the drag force along a single projection (Eq. 2). On the other, one could treat the projections as an ‘effective porous medium’ (13, 14) that results in an altered flow profile. The first is more applicable for a sparse array of projections (e.g. primary cilia in tubules), while the second is more applicable for a dense array, such as the brush border.

If we consider the projections to be an effective medium, one simply adds a ‘Darcy term’ (15) to the Navier-Stokes equations, and considers the effect on the fluid velocity to be formally identical to a frictional force with a constant of proportionality ‘k’ which has units of viscosity/area. The identity of ‘k’ is currently unknown, but will be calculated later.

$$\text{Eq. 6. } 0 = -\frac{dP}{dz} + \mu \nabla^2 U - kU.$$

Again, for steady state flow through a cylindrical tube, assuming the velocity is only along the tubule axis, one obtains the differential equation (the Brinkman equation):

$$\text{Eq. 7. } 0 = -\frac{\partial P}{\partial z} + \mu \left[\frac{1}{r} \frac{\partial}{\partial r} \left(r \frac{\partial U}{\partial r} \right) \right] - kU.$$

The solution to this equation is more complex than simple Poiseuille flow, but is still easily solved:

$$\text{Eq. 8. } U(r) = C_1 I_0 \left(\sqrt{\frac{k}{\mu}} r \right) + C_2 K_0 \left(\sqrt{\frac{k}{\mu}} r \right) - \frac{1}{k} \frac{dP}{dz}$$

whereby C_n = constants of integration, I_0 and K_0 = modified Bessel function of the first and second kind, respectively, of order ‘0’ and other symbols are as defined previously.

Finally, we match the effective medium solution above (Darcy flow) to the unperturbed Poiseuille flow solution at the tip of the brush border. That is, for R = tubule radius, δ = microvillus length, and r = radial coordinate, Poiseuille flow holds from the center of the tubule ($r = 0$) to the top of the brush border ($r = R - \delta$), and Brinkman or Darcy flow holds in the region from the brush border to the wall ($r = R$).

Mechanical stimulation of primary cilia

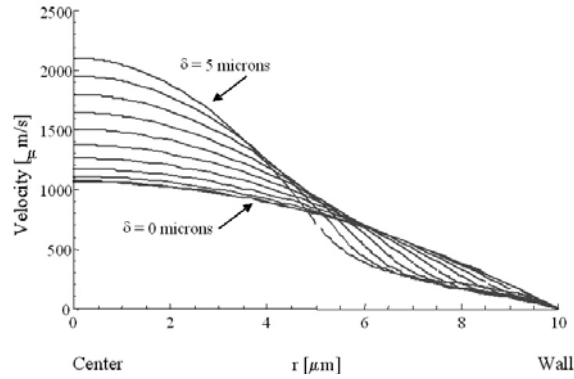


Figure 2. Change of flow profile due to obstruction by brush borders of height (δ), varying between 0 (no obstruction) and 5 μm in increments of 0.5 μm . The velocity distribution $U(r)$ has been calculated for a constant volumetric flux of 10 nl/min within an obstructed 10 μm diameter tubule and a frictional constant ' k ' numerically equal to the fluid viscosity.

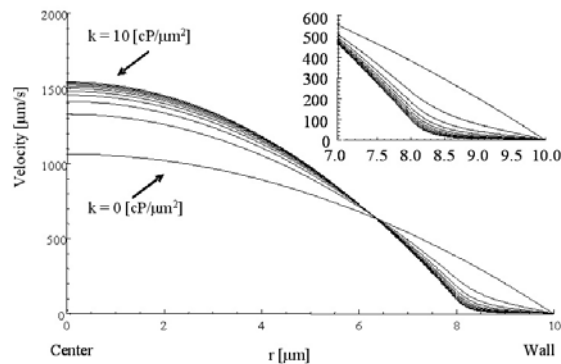


Figure 3. Change of flow profile due to Darcy frictional resistance ' k ', varying between 0 (pure Poiseuille flow) and 10 $\text{cP}/\mu\text{m}^2$ in increments of 1 $\text{cP}/\mu\text{m}^2$. The velocity distribution $U(r)$ has been calculated for a constant volumetric flux of 10 nl/min within an 10 μm diameter tubule obstructed by brush borders with a height of $\delta = 2 \mu\text{m}$. The inset is the region near the wall, where the brush borders are.

$$\text{Eq. 9a Poiseuille region: } \begin{cases} \frac{dP}{dz} = \mu \left[\frac{1}{r} \frac{\partial}{\partial r} \left(r \frac{\partial U_1}{\partial r} \right) \right] \\ U_1(r) = \frac{dP}{dz} \frac{1}{4\mu} r^2 + C_1 \end{cases}$$

$$\text{Eq. 9b Brinkmann region: } \begin{cases} \frac{dP}{dz} = \mu \left[\frac{1}{r} \frac{\partial}{\partial r} \left(r \frac{\partial U_2}{\partial r} \right) \right] - k U_2 \\ U_2(r) = C_3 I_0 \left(\sqrt{\frac{k}{\mu}} r \right) + C_4 K_0 \left(\sqrt{\frac{k}{\mu}} r \right) - \frac{1}{k} \frac{dP}{dz} \end{cases}$$

Because of the mathematical complexity, this “matched” solution must be presented in a separate paper.

We have solved this system of equations and provide a few plots of the complete interior solution for various values of the parameters ' δ ' and ' k '.

Figure 2 shows the velocity profile for various values of the length of microvilli or cilia (δ) with the friction coefficient ' k ' set numerically equal to the viscosity. The plot is with Q_V held constant. What is seen is that the velocity in the center of the tubule grows extremely fast, for even small changes in the brush border height. Thus, it is possible that the brush border height could be controlled by a flow sensor that protrudes further into the central region of the tubule- for example, the primary cilium.

Figure 3 shows the velocity profile for various values of the friction coefficient ' k ' with δ held constant at 2 μm , keeping also the volume flow Q_V constant. It is seen that the peak velocity grows while the velocity within the Brinkman region decreases as ' k ' increases. A detailed view of the Brinkmann region is shown in the inset. This indicates that cellular regulation of the value of ' k ' will have effects on flow.

For motile cilia, the cilium exerts a force on the fluid, which induces a flow. Conceptually, we can simply allow the parameter ' k ' in Eq. 6 to become negative. Dillon and Fauci (16) present a model where F_b is determined from the structure of the axoneme and movement of motor proteins. Allowing ' k ' to assume negative values is known as “negative friction” (17), and so our approach can be considered a macroscopic description of the microscopic model presented by Dillon and Fauci.

Although not widely known, negative friction systems are well-characterized. The system must be coupled to a reservoir of energy, and some experimental realizations do exist. If we hypothesize that a possible energy reservoir is due to motile cilia (airway cilia, oviduct, etc) imparting motion to the fluid, those particular ducts could potentially be modeled in terms of negative friction. We include a plot (Figure 4) showing the effect of negative friction (negative values of k), with $\delta = 2 \mu\text{m}$ and volumetric flow held constant. It should be pointed out that the solution rapidly becomes unstable even for moderate values of ' k ', and so it is not clear if this implies the action of the motile cilia are tightly regulated, or if the theoretical approach is simply not applicable. In any case, the effect of ‘negative friction’ is to increase the velocity near the tubule wall and decrease the centerline velocity.

3.5. Evaluation of ' k '

We have left ' k ' undefined up until now for reasons of clarity. Now we will present a value for ' k ' based on the area fraction of cylindrical projections. We will present values of ' k ' for hexagonal arrays of projections and apply the theory to measured data as well.

Sangani and colleagues (18, 19) have studied viscous flow through hexagonal and random arrays of infinite cylinders. They derived a relationship between the

Mechanical stimulation of primary cilia

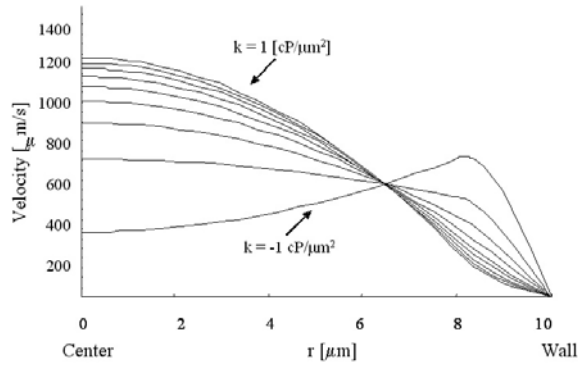


Figure 4. Change of flow profile due to negative values of the Darcy frictional resistance 'k', which occurs when motile cilia impart velocity to the fluid. The velocity distribution $U(r)$ has been calculated for a constant volumetric flux of 10 nl/min within an 10 μm diameter tubule obstructed by brush borders with a height of $\delta = 2 \mu\text{m}$. 'k' has been varied from -1 to 1 $\text{cP}/\mu\text{m}^2$ in steps of 0.25.

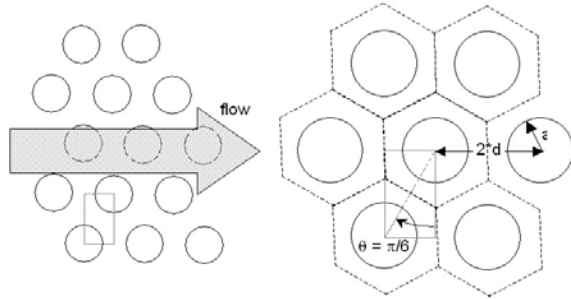


Figure 5. Geometry of obstructed tubule flow. The view is along the radial axis of the tubule, along the axoneme of the projections (cilia, microvilli). Flow is perpendicular to the axonemes. The projections are arranged in a hexagonal crystalline array, and a unit cell is highlighted. a = radius of cylindrical projection, $2d$ = distance between projections, θ = smallest angle of the triangle formed by diagonal and sides of a unit cell.

average pressure drop (equivalently, the average velocity) per unit length (transverse to the projection axes) and the resultant drag force per unit length (along the projection axis) exerted on a single cylinder. Figure 5 shows the geometry for a hexagonal array of cylinders based on a unit cell with cylinder radius of 'a' and cylinder center-to-center distance of $2d$. Thus, in order to calculate the drag force, the center-to-center distance between projections must be measured or calculated.

One may reasonably ask why this model should be applied to a proximal tubule. The answer is that an infinite array of cylinders is a reasonable first approximation to the brush border elements: microvilli have an aspect ratio (length/radius) of approximately 50. The fact that the tubule velocity varies along the height of the brush border does not disqualify this model either, because 'k' is independent of fluid velocity.

Sangani *et al.* begin with the average pressure drop due to the cylinder within a unit cell

$$\text{Eq. 10} \quad \frac{dP}{dz} = \frac{-nf}{A},$$

where n is the number of cylinders per unit cell, ' f ' the drag force per unit length, and A the area of the unit cell. Darcy's law (15) is an empirical law for creeping flow through a porous medium, and is expressed as:

$$\text{Eq. 11.} \quad \frac{dP}{dz} = -\frac{\mu}{K}U$$

where K is the permeability of the porous medium.

Dimensional analysis shows that $K = \frac{\mu}{k}$, and so Darcy's

law can also be written as $\frac{dP}{dz} = -kU$, which is identical to what we have written above in Eq.6 - recall for Darcy flow, the viscous term ($\nabla^2 U$) is very small and can be neglected.

$$\text{Equating the two expressions for } \frac{dP}{dz} \text{ gives } K = \frac{\mu U}{nf} A$$

$$\text{or } \frac{k}{\mu} = \frac{nf}{\mu U} \frac{1}{A}.$$

$$\text{For a hexagonal array, } \frac{k}{\mu} = \frac{f}{\mu U} \frac{1}{2A}, \text{ whereby } A$$

refers to the area of a unit cell as shown in Figure 5 and which includes only half of a cylinder cross-sectional area. The permeability 'K' was computed for hexagonal (18) and random (19) arrays as a function of area fraction occupied by cylinders $\phi = \frac{n\pi a^2}{A}$. Experimentally, what is measured

is not the number of projections per unit cell 'n' but rather the projections per unit area ξ . If the projections are arranged as a regular array, each projection has an assigned area of $1/\xi$. If they are arranged as regular hexagons, the center-to-center distance $2d$ is related to other parameters as follows: $\frac{1}{\xi} = 6d^2 \tan\left(\frac{\pi}{6}\right) = 2\sqrt{3}d^2$, the area fraction

$$\phi = \frac{\pi}{2\sqrt{3}} \frac{a^2}{d^2}, \text{ and } \frac{k}{\mu} = \frac{f}{\mu U} \frac{\phi}{\pi a^2}.$$
 We may now

substitute the various derived expressions for $\frac{f}{\mu U}$ to

obtain values for k . For the hexagonal array the maximal

area fraction ϕ_{max} is $\frac{\pi}{2\sqrt{3}} = 0.9069$, and the scaled

area fraction is $\chi = \phi/\phi_{\text{max}}$.

Mechanical stimulation of primary cilia

Table 2. Values for Darcy's resistance term 'k' for tubules partially occluded by a brush border

| Experimental condition | MV density [# per μm^2] | 2d [nm] | ϕ | χ | $f/\mu U$ [dimensionless] | k [cP/ μm^2] |
|------------------------|-------------------------------------|---------|--------|--------|---------------------------|--------------------------|
| Low flow | 49.9 | 152 | 0.318 | 0.350 | 140 | 4200 |
| control | 42.5 | 164 | 0.273 | 0.301 | 109 | 2800 |
| High flow | 35.5 | 180 | 0.226 | 0.249 | 84 | 1800 |

Microvilli. Microvillus (MV) density obtained from Maunsbach *et al.* (20). 2d = average distance between neighboring microvilli; ϕ = projected area fraction occupied by microvilli; χ = scaled area fraction occupied by microvilli (see text); f = force per unit length; μ = fluid viscosity; U = axial velocity. The radius of microvilli is taken as 45 nm.

We have the following cases:

Dilute array:

Eq. 12a.

$$\frac{f}{\mu U} = \frac{4\pi}{Ln(\chi^{-1/2}) - 0.745 + \chi - 0.25\chi^2}$$

Concentrated array:

Eq. 12b.

$$\frac{f}{\mu U} = \frac{27\pi}{4\sqrt{2}}(1 - \chi^{1/2})^{-5/2}$$

“dilute” means that $\chi < 0.2$, while “concentrated” holds for $\chi > 0.3$.

For tubules with only primary cilia ($r=0.1 \mu\text{m}$, $d=10 \mu\text{m}$), χ

$$= \frac{\pi}{2\sqrt{3}} \left(\frac{0.1}{10} \right)^2 = 1 \cdot 10^{-4} \text{ giving } \frac{f}{\mu U} \sim 3 \text{ and } k \sim$$

$5 \cdot 10^{-3} \text{ cP}/\mu\text{m}^2$. Thus in the Loop of Henle and collecting duct, we have essentially undisturbed Poiseuille flow, as we expect.

For the brush border of the proximal tubule, k can be estimated from the density of microvilli and their radii. Table 2 presents k values based on the data by Maunsbach *et al.* (20). As expected, the Darcy resistance term 'k' is relatively high with values greater than 1,000 cP/ μm^2 . Such values for 'k' show that the brush border exerts an appreciable effect on the flow distribution (refer to Figure 3). Interestingly, the k value is higher at lower flow rates, but this could be an in-vitro artifact due to the experimental conditions of perfused excised tubules: As the tubule wall is compliant, isolated, perfused tubules can expand with increasing pressure and flow rate, while in vivo, the tubules are constrained against expansion by other surrounding tubules. The flow velocities in the unobstructed portion of the lumen are significantly higher than if the brush border was not present.

3.6. Further developments in the model

One approach is to simply add complexity to this model as desired. For example, as the microvilli flex, the height of the Darcy layer changes. We may choose to model the entire tubule, and perhaps digitize a casting of an excised tubule to obtain the shape of the lumen. We may add the effects of fluid resorption, wall compliance, or any number of additional refinements. The relevant issue is the accuracy of predictions made by any model, and if adding complexity gains an appreciable increase in predictive power.

Conceptually however, some outstanding issues remain which should be resolved prior to increasing the model complexity. As mentioned above, micropuncture data on the intratubule pressure is difficult to interpret and reconcile, given the many biological processes that modulate the hydraulic pressure within a nephron (4-6, 21). Also, there is no data on the intratubule pressure or flow rates along interior portions of the nephron- the loop of Henle, for example. Thus at present, there is at best an incomplete understanding of the *in vivo* mechanical environment of the primary cilium.

Biology and biochemistry are also required to inform the further development of the physical model. As examples, it would be interesting to determine if there is a definite ratio between microvilli and ciliary length in the proximal tubule. An ultrastructural study could check to see if there is a change in cilium length with severe tubule obstruction. Measurements of fluid velocity in the oviduct could determine if and how much motile cilia contribute to the fluid movement. The collecting duct system could be artificially occluded, and upstream regulators of water and salt transport could be analyzed.

It is important to keep in mind, however, that determination of the flow rate is not the primary goal here. Rather, the flow rate determines the force incident on a cilium, and determination (and manipulation) of this force is the primary goal.

Let us be clear about what we have done; derived a simple model for the *in vivo* flow through a tubule containing cilia and possibly a brush border. We have done this simply because experimental manipulations of cilia need to be placed in the context of physiological conditions, and this requires a rational framework to compare disparate measurements.

4. IN VITRO APPROXIMATIONS FOR $U(r)$

The goal of the above section was to develop a model for the *in vivo* flow conditions and *in vivo* forces incident on a cilium. We now turn to *in vitro* experimental approximations.

4.1. Flow chamber

Perhaps the most obvious method to approximate *in vivo* conditions is to culture the cells in a flow chamber (22-25), or even to perfuse isolated tubules (26-28). In that case, the sections above still apply and the experimenter can control Q_v to generate a wide range of mechanical forces. The current experimental difficulty is culturing polarized cells (for example, epithelial cells), in a flow chamber containing cells on a permeable support. There

Mechanical stimulation of primary cilia

does not yet appear to be a commercial solution to this problem.

4.2. Body forces on a cilium

Going back to Cauchy's first law (Eq.

$$\rho \frac{DU}{Dt} = \nabla \cdot T + F_b$$

3) , we previously mentioned that F_b is a 'body force' term and used friction ($-kU$) as a body force. We must be careful to distinguish between a static equilibrium achieved by application of a (steady) body force and fluid flow created by a varying body force, which then acts on the cilium via drag. Here, we are concerned with static configurations- equilibrium fluid shape, static cilium shape, and it is important to realize under what experimental conditions this occurs.

Another force is buoyancy, which acts to create a net force between regions of different density $F_b = \Delta\rho g$, where $\Delta\rho$ is the density difference between the cilium and the surrounding fluid and 'g' the gravitational acceleration. Gravitational effects on cell function are currently being studied in the context of lunar and interplanetary travel, especially in regards to bone remodeling (29). This problem is complicated by fluid flow that results from movement- it is not clear if the cells are sensing gravity per se, or the resultant fluid flow.

However, gravity is not the only way to exert a force via density differences. We may attempt to mimic the drag force produced by flow by applying an acceleration to the cell directly. Any uniform force will act differently on regions of different density, and so the net force caused by rotation, circular motion or vibration could all accelerate a cilium with respect to the surrounding fluid. For example, placing cells on a turntable or centrifuge will induce a net force of $\Delta\rho\omega^2r$, where r is the distance to the center of rotation and ω the rotation frequency. This force is directed radially, and so depending on the orientation of the cells, the force will act either perpendicular to the cilium or along the axoneme axis. Because the cilium is anchored at the basal end, one can easily picture that the cilia experience an 'outwardly' directed force and achieve a static, bent configuration even in the absence of fluid flow.

Similar expressions can be written down for linear vibrations of amplitude A and frequency ω : $F_b(t) = A\Delta\rho\omega^2\sin(\omega t)$, or $A\Delta\rho\omega^2/2$ for the time-averaged expression. Again, depending on the orientation of the oscillation with respect to gravity, the vibration can act in concert with or perpendicular to gravity, and can act transverse or axially, depending on the orientation of the cilium.

For orbital motion with a throw distance R and frequency ω , the force is written as $F(t) = \Delta\rho\omega^2 R [\hat{x} \cos(\omega t) + \hat{y} \sin(\omega t)]$. Averaged over time, this simply equal to $F_b = \Delta\rho\omega^2 R$, the same as centripetal force. The primary difference is that the centripetal force varies with distance from the center of rotation, while for orbital motion, the force is constant. We

have shown (2) that orbital motion induces fluid flow through interaction of the fluid with the rigid walls of a partially-filled culture container.

Estimating the cilium contents as 20% protein (1.4 g/cm³), 5% carbohydrates (1.6 g/cm³), 75% lipids/water (1.0 g/cm³) gives an averaged uniform cilium density = 1.11 g/cm³. Because of the small size and density difference between cilium and fluid, it is expected that *in vivo*, body forces are much smaller than fluid drag forces. What emerges are two limiting cases for experimental conditions: i) a steady acceleration is applied (e.g. centrifugation) which eliminates flow effects while applying a meaningful force to the cilium due to the density difference between the cilium and fluid; and ii) a small time-varying acceleration is applied, resulting in a time-varying induced fluid flow which then exerts drag onto the cilium. Using the *in vivo* flow conditions calculated above, experimental conditions can be tuned to match a range of expected incident forces.

Finally, it is possible to apply a force to a cilium by direct contact- for example, by application of a microneedle to mechanically deflect the cilium (23, 24, 30, 31). The final deformation state of the cilium depends on both the point of contact and the amount of force transmitted. Thus, it is expected that accurate and repeatable results will be obtained only if those particular details are unimportant.

Now if a force acts on a cilium and it moves through the surrounding fluid, there will be, by necessity, a flow induced by the motion of the cilium which then acts on either neighboring cilia (hydrodynamic coupling), or back on the cilium itself via viscous drag. This problem will not be addressed here.

4.3. Optical tweezer

The development of optical tweezers as a tool to manipulate microscopic particles began in the early 1970's with the use of a focused laser beam to levitate transparent spheres (32-35). Optical tweezers found their first application within the field of biology to manipulate single cells (36, 37) as well as subcellular structures (38). Laser tweezers have found a use in biology chiefly because optical trapping is a non-contact method of exerting a force on live cells and the magnitude of force applied (fN to ~100 pN) (39) is appropriate for the cellular and subcellular scale.

Related to optical tweezers are magnetic tweezers, which use a magnetic field and paramagnetic beads to exert forces. Magnetic tweezers require lower energy levels to operate, and photodamage is not a problem. In addition, the force can be applied in a time-dependent way that is much more general than typically found with laser tweezers. However, paramagnetic beads must be used to transduce a force, and the spatial precision of magnetic tweezers is lower than optical tweezers. In both cases, use of functionalized beads has allowed investigation of a variety of biological phenomena (40-42).

Mechanical stimulation of primary cilia

4.3.1. Principles of laser tweezer operation

The theory of optical tweezers has been extensively published in the literature (43-45), and so a detailed derivation will not be presented here. Optical tweezers work by creating a potential well due to the spatial gradient of the electromagnetic field. While the specific forces involved are well understood, their analytic expression remains problematic. To overcome the restrictions involved, it is possible to instead consider optical trapping forces derived from Mie scattering theory (46). The series expansions for the electric field E and magnetic field H are standard Mie calculations, and solved in the typical way. The key is then to provide a correct formulation of the incident beam. This is not trivial, but significant progress has recently been made (47-50), with spherical aberration (48, 49) being a notable component of the formulation.

Consequently, laser tweezers must be calibrated in some way, much like a glass microneedle is calibrated. When trapping a cilium or even a microsphere, it is not realistic to calculate the applied force *ab initio*. It should be noted that the ability to trap particles does not rely on the absorption of light- the force is created by scattering the incident field. This is the origin of the theoretical problem, as the scattering of light by particles of arbitrary shape and composition is not, in general, analytically solvable.

4.3.2. Biological considerations

Other than photodamage concerns (51, 52), which relates to the laser wavelength and maximal power, the main choice faced by an experimenter is on what to apply a force to- one may either trap a cilium directly or instead, trap a microsphere that is bound to a cilium via some functionalization of the microsphere surface.

4.3.3. Trap strength measurement

Properly speaking, the laser tweezer applies a restoring force only to a particle that is displaced from the center of the trap. Thus, the correct way to quantify the trap is by a spring constant (53), or since the particle is confined in three dimensions rather than one, some generalization of a spring constant. There are two commonly accepted methods to simplify the characterization of a laser trap. One case uses a known particle, a known fluid, and a simple measurement of the trap geometry, (54, 55) while the other tracks a trapped particle and compares the behavior of the particle with one that experiences Brownian motion.

4.4. Summary of *in vivo* and *in vitro* models

We have so far operated on the assumption that ciliary-initiated signaling processes could occur without a specific biochemical initiator. For example, ligand-receptor binding events are not required to initiate a signaling event. It is not clear that any experiment has been performed to separate the putative mechanotransduction mechanism from a possible chemotransduction mechanism. Additionally, mechanotransduction experiments typically compare a flow-mediated response with a no-flow condition; this is very different from comparing cellular

responses to two different flow conditions. Finally, experiments to date have not consistently separated force effects on a cilium from force effects on the cytoskeleton or apical membrane. Thus, isolating the seat of mechanotransduction to the cilium has been problematic.

We have endeavored here to model physiological flow conditions in tubules. The flow contains information about organ and organism function (or dysfunction), and so the hypothesis that the flow is monitored to regulate function and health is reasonable. Flow can be monitored either chemically or mechanically, and it is reasonable to assume that a sophisticated regulatory system would monitor both. The next question to be resolved is how the flow interacts with the cilium, which is the subject to which we now turn.

5. BENDING OF A CILIUM

Some basic questions regarding cilia-mediated mechanotransduction remain. First, is the process static (i.e. dependent on the shape of the cilium) or dynamic (depending on the rate of change)? Because flow in the renal tubule is at least quasi-static, we hypothesize that mechanotransduction can occur in a static situation. It should be noted that under this hypothesis, the deformed shape of the cilium is not important per se, but rather the strain energy contained in the cilium as a result of the deformation. Thus, the kinetic energy contained in the fluid flow is transduced, via the drag, to strain energy in the cilium via compressive and tensile strain. This strain energy could then be transduced, for example, via strain-sensitive membrane proteins into a biological function, such as transepithelial sodium current (2, 56), protein cleavage and translocation (56) at the cellular level, or control of cell orientation (57) during cell division at the organ level.

In this section, we will model bending of cilia by fluid flow and the associated strain energy. The modeling is based on experimental data of cilium length and fluid velocity at some point along the cilium length, which is necessary to calculate the drag force, as well as measured ciliary deflections for these conditions. The ciliary deflection by a known drag allows one to calculate the bending rigidity of cilia. Only small deflections are considered because then the fluid drag force remaining perpendicular to the cilium axis can be approximated. Again, the modeling is based on the assumption that the cilium can be described as a circular cylinder of uniform diameter and mechanical properties, i.e., that it is essentially homogeneous in composition. Comparison with previous work is problematic for two reasons: First, a wide range of values have been presented for the bending (flexural) rigidity of cilia (58-61). Second, previous work has omitted the drag contribution from the endcap – whether a simple hemisphere or large “balloon” protrusion. This contribution constitutes close to 50% of the total drag force on a cilium (2). Our modeling assumes $31 \text{ pN}\cdot\mu\text{m}^2$ for the ciliary bending rigidity, a value supported by more data than others from the previous literature.

Mechanical stimulation of primary cilia

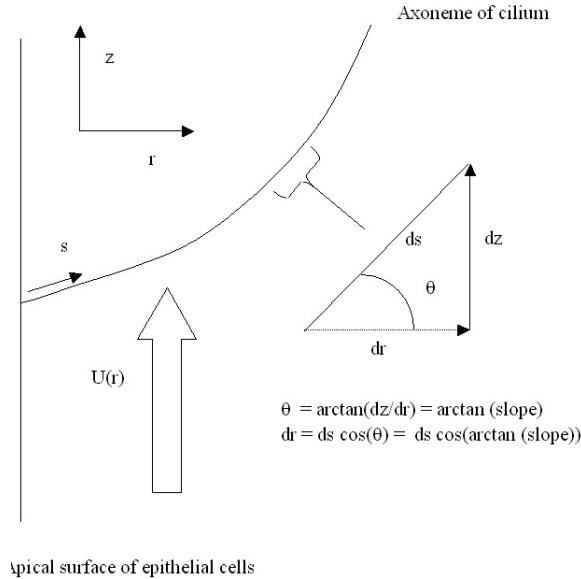


Figure 6. Schematic of cilium deformation geometry. The coordinate 's' runs along the axoneme, and the projection of cilium length 'dr' transverse to the flow direction in terms of the local slope is given.

The description of ciliary bending requires calculations of degree of bending and force in terms of the coordinate 's' that runs along the axoneme rather than the radial (laboratory) coordinate 'r'. The bending of a slender cylindrical rod under the influence of a distributed force in the z-direction is given for the steady-state by Segel (3) as follows:

$$\text{Eq. 13 } EI \frac{\partial^4 z}{\partial s^4} = f(s)$$

where EI describes a mechanical property of the cilium and is referred to as 'flexural rigidity' with units of 'force*area'. EI is the product of 'E', Young's modulus of the cilium (rod), and 'I', the second moment of inertia.

'I' can be calculated for a cylinder of radius 'a':

$$\text{Eq. 14 } I = \frac{\pi}{4} a^4$$

The contribution from the end cap is treated as a concentrated load at the free end of the cilium. The drag force $f(s)$ for Poiseuille flow in terms of the coordinate 's' is given by Eq. 1.

The structure of a cilium and basal body justifies using the boundary conditions for a cantilevered rod with a built-in end when solving Eq. 13. There is no analytical solution for Eq. 13 using Eq. 1, but the problem can be readily solved numerically. A trickier problem is properly calculating U(s), given that the fluid velocity is specified above in terms of the laboratory coordinate 'r'. In order to

do so, one must convert the deformed coordinate back to the laboratory coordinate. Figure 6 shows the geometry of the problem. The conversion is accomplished by the transformation:

$$\text{Eq. 15a } r(s) = \int_0^L \cos \left(\arcsin \left[\frac{dz}{ds} \right] \right) ds$$

which is intrinsically nonlinear. It is important to remember that for small deflections, 'r' essentially coincides with 's'. What we have done is to linearize the problem by considering small deflections (ratio of tip deflection to cilium length is less than 0.4) and considering only the component of the drag force acting transverse to the axoneme. Note that our solution is slightly different from that used Schwartz *et. al.* (60). Our approximation changes Eq 15a slightly, to

$$\text{Eq. 15b } r(s) = \int_0^L \cos \left(\arctan \left[\frac{dz}{dr} \right] \right) ds$$

And we linearly approximate the function $\cos(\arctan(x))$ by $(1-0.3*x)$, which is reasonably valid for slope values less than 2. Deformation of the cilium by both a distributed drag force and concentrated load from the endcap is thus approximated by the following system of equations:

$$\text{Eq. 16a } EI \frac{\partial^4 z}{\partial r^4} = \frac{4\pi\mu U(r)}{\frac{1}{2} - \gamma - \ln \left[\frac{2aU(r)}{8\nu} \right]} \left(1 - 0.3 * \frac{\partial z}{\partial r} \right)$$

$$\text{Eq. 16b. } z|_{r=0} = 0$$

$$\text{Eq. 16c } \frac{\partial z}{\partial r} \Big|_{r=0} = 0$$

$$\text{Eq. 16d } \frac{\partial^2 z}{\partial r^2} \Big|_{r=L} = 0$$

$$\text{Eq. 16e } EI \frac{\partial^3 z}{\partial r^3} \Big|_{r=L} = 3\pi\mu a U(L)$$

Figure 7 shows modeling results based on the above equations. Specifically, ciliary deflections were calculated for different tubule diameters when the volumetric flow and cilium length were held constant. The deflection is significantly greater with decreasing tubule diameter due to increased flow velocity. This result suggests that ciliary deflection could play a role in feedback mechanisms that regulate tubule diameter relative to volume flow, e.g., during development.

Figure 8 illustrates the effect of ciliary length on bending at constant flow and demonstrates that the degree of bending increases significantly with length. This is an important result because ciliary length can be biologically regulated and hence the sensitivity to bending adjusted.

Mechanical stimulation of primary cilia

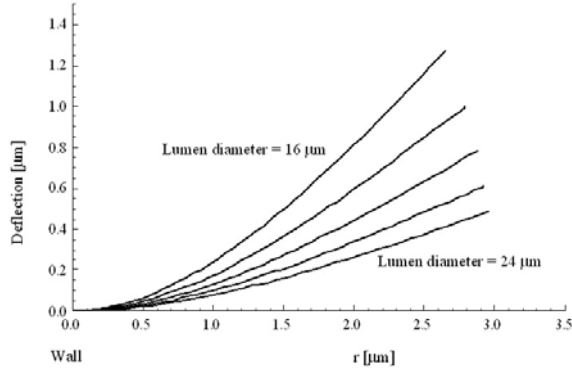


Figure 7. Effect of tubule diameter on deformation of a 3 μm long cilium. Shown are the equilibrium shapes of a cilium immersed in Poiseuille flow at constant volume flow (45 nl/min), but different tubules ranging in diameter from 16 to 24 μm . Small changes in the diameter of the tubule (or velocity within the tubule) result in large changes in the cilium deflection. The flexural rigidity of the cilium is taken to be 31 $\text{pN}\cdot\mu\text{m}^2$.

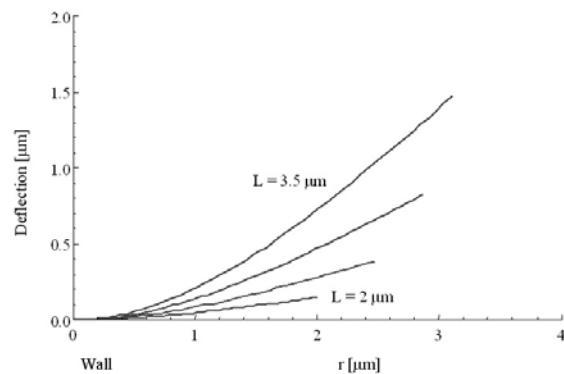


Figure 8. Effect of cilium length on cilium deflection. The volumetric flux is held constant at 45 nl/min, the tubule diameter held constant at 20 μm , and the cilium length is varied between 2 and 3.5 μm . Small changes in the length of the cilium result in large changes in the cilium deflection. The flexural rigidity of the cilium is taken to be 31 $\text{pN}\cdot\mu\text{m}^2$.

The curvature of a bent cilium indicates strain on one side and compression of the other. The strain energy is proportional to the curvature, i.e., the square of the second derivative. The strain energy per unit cilium length (\mathcal{E}) is given by:

$$\text{Eq. 18} \quad \mathcal{E} = \frac{1}{2}EI \left(\frac{\partial^2 z}{\partial r^2} \right)^2$$

Calculations of the strain energy for the conditions of Fig.8 are shown in Figure 9. They demonstrate that, even in the case of slow flows, the strain energy density is highest at the basal end of cilia. In other words, the strain energy resulting from fluid drag is localized at the ciliary base, even though the applied force

is distributed along the entire length of the cilium with a major contribution by the free endcap, where fluid velocity is highest. The plotted strain energy represents an upper limit of what is available for strain-sensitive proteins. Interestingly, the ciliary location of the proteins polycystin-1 (22), polycystin-2 (62), and P100 (56) are predominantly at the base or basal body. Polycystin-1 and -2 form a complex and defects in either protein are associated with polycystic kidney disease (63). Based on the coincidence of the strain distribution and protein location in cilia, a logical hypothesis is that polycystins, at least when they exist as complex, are strain-sensitive and mediate the sensation of fluid flow to the cell. Sensitivity of such a flow sensor could be adjusted by altering ciliary length, as discussed above.

Next, we include the effect of a brush border on ciliary bending in our modeling. The simultaneous presence of a brush border and cilium represents a situation encountered in the proximal tubule. In Figure 3, the velocity profile was modeled for a tubule partially occluded by brush border. The cross section is divided into a central, unobstructed Poiseuille region and a peripheral Brinkmann region containing the brush border, whereby the flow profile is described by Eqs. 8a plus 8b. Figure 10a illustrates the velocity profile for realistic parameters of proximal tubules with or without a brush border. Figure 10b illustrates the corresponding deformation profile of cilia that rise from 1 to 6 μm above the brush border. Interestingly, short cilia are bent less and long cilia more in presence of a brush border because of the altered flow profile with faster central flow. For the conditions of Figure 10, reversal from decreased to increased bending occurs for cilia between 4 and 5 μm . This result again suggests that cells could regulate flow sensitivity of cilia by adjusting cilium length.

Schwartz *et al* (60) have published flow velocities and length and curvatures of cilia in a rat kangaroo kidney epithelial cell line. We have used their (Table 1) data to estimate the flexural rigidity EI of cilia using the equations 17. The new estimates of EI are presented in the right-most column of Table 3, together with the corresponding experimental data from Schwartz *et al.* on which they are based (see Table for details of the fitting and inherent assumptions). The mean value for EI is 21 $\text{pN}\cdot\mu\text{m}^2$ with a range between 1.8 and 350 $\text{pN}\cdot\mu\text{m}^2$. These results are similar to the estimates by Schwartz *et al.*, which ranged between 14 and 51 $\text{pN}\cdot\mu\text{m}^2$ depending on method for calculation, although the variance based on our calculations is much greater than that of Schwartz *et al.*. The reason for this discrepancy is not clear at this point. It could be related to inclusion of the drag force at the cap by us. In any case, no error estimates of the primary measurements and error propagation calculations with respect to the flexural rigidity have been carried out. This lack of information, together with the relatively wide range of calculated data, indicates that better quantitative measurements still need to be carried out. Such measurements would be necessary to determine the energy available to drive biochemical processes.

Mechanical stimulation of primary cilia

Table 3. Flexural rigidity (EI) of non-motile cilia

| Experiment | Cilium length [μm] | Tip deflection [μm] | Tip velocity [$\mu\text{m/s}$] | Flexural rigidity [$\text{pN}\cdot\mu\text{m}^2$] |
|------------|---------------------------------|----------------------------------|----------------------------------|---|
| 1 | 13.2 | 4.5 | 6 | 1.8 |
| 3 | 11.0 | 2.3 | 56 | 22 |
| 4 | 17.3 | 2.1 | 135 | 350 |
| 5 | 11.4 | 5.0 | 195 | 32 |
| 6 | 17.1 | 10.5 | 86 | 16 |
| 7 | 18.4 | 9.5 | 47 | 19 |
| 8 | 14.7 | 5.7 | 43 | 16 |

Calculated from the data in Table 1 of Schwartz *et al.*, (60) for cilium length, tip deflection, and tip velocity. Calculations are based on solving Eqs. 17 by allowing EI to vary until the calculated tip deflection matched the measured one. The table includes all experiments from Schwartz *et al.* for which the slope at the tip was less than 2, as only this range is valid for Eqs. 17. After omission of 2 outliers, the mean \pm standard deviation of the flexural rigidity calculates as $21 \pm 7 \text{ pN}\cdot\mu\text{m}^2$. This value is comparable to the widely accepted value of $31 \text{ pN}\cdot\mu\text{m}^2$ in the literature, i.e., the mean + (1.3 standard deviations) = $31 \text{ pN}\cdot\mu\text{m}^2$. Note that the range of calculated values is large (~ 200 -fold). The reasons for this are unclear, but are not due to uncertainties in EI due to the fitting procedure. It was determined that the fractional error in EI (standard deviation/mean) is 5% based on multiple independent attempts at fitting.

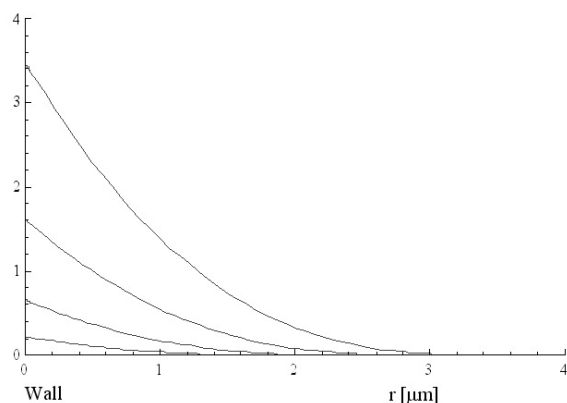


Figure 9. The distribution of stress along the axoneme. The plot shows the deformation energy per unit length for cilia of different lengths as a function of position along the axoneme. Tubular flow is held constant at 45 nl/min, tubule diameter at $20 \mu\text{m}$, and flexural rigidity of the cilium at $31 \text{ pN}\cdot\mu\text{m}^2$, while the cilium length is varied between 2 and $3.5 \mu\text{m}$. Note that the stress is maximal at the base of the deformed cilium.

6. PERSPECTIVE

It is instructive to recall what the purpose of this manuscript is: to develop a model for the *in vivo* environment of a primary cilium, and *in vitro* approximations to that environment. The model we have presented here is a steady-state model, corresponding to chronic conditions. Thus, it is expected that experiments involving developmental biology or wound healing would be most instructive to show under what conditions the model fails. Additionally, in the airway where there is unsteady flow imposed in addition to motion induced by the motile cilia, the model is expected to fail completely.

As an example experiment, calcium waves are set off by touching cilia (30). The relevant biological input to the model above would be if the calcium wave is initiated by (acute) cilium motion, or if steady-state static

deformation is the cause of intracellular Ca^{2+} release. This could be performed by observing the intracellular Ca^{2+} concentration under a range of bending rates, or by long-term observation in the presence of steady flow.

7. BIOLOGICAL EFFECTS

Other manuscripts in this volume will no doubt cover this topic in detail, so we simply provide a summary of the various cilia-mediated biological actions in an effort to bridge the physical model with biological models.

7.1. Cellular-level effects

One acute cellular-level response is clearly intracellular Ca^{2+} release (22, 23, 26). However, many signaling pathways (AT1 (64), STAT (56), wnt (65) and TRPV4 (66)) have been shown to be activated by the bending of a cilium, and several proteins (PC1/PC2 (22), Shh (67)) have been shown to become functional when a cilium is bent. We have shown that transepithelial sodium transport is also changed in response to ciliary bending (2). Thus, clear evidence showing that the deformed state of a cilia initiates cellular processes exists, and the hypothesis that fluid flow provides the ciliary deformation is reasonable.

7.2. Organ-level effects

In kidney, liver, and pancreas, clear evidence showing a link between ciliary dysfunction and cyst formation exists (68-71). Additionally, organ-level cellular organization (tubule growth) has been shown to be cilium-dependent (72). Planar cell polarity signaling has a ciliary dependence (57). Organ level diseases caused by faulty cilia include nephronophthisis (73), retinal degeneration (73, 74) and hydrocephalus (75).

7.3. Organism-level effects

Similarly, at the organism level, there are several diseases caused either by dysfunctional cilia or by proteins associated with cilia. These include primary ciliary dyskinesia (73), hypertension (76), Senior-Løke syndrome, Joubert syndrome, situs inversus (73), Bardet-Biedl syndrome (73, 77), Alstrom syndrome and Meckel-Gruber syndrome (73).

Mechanical stimulation of primary cilia

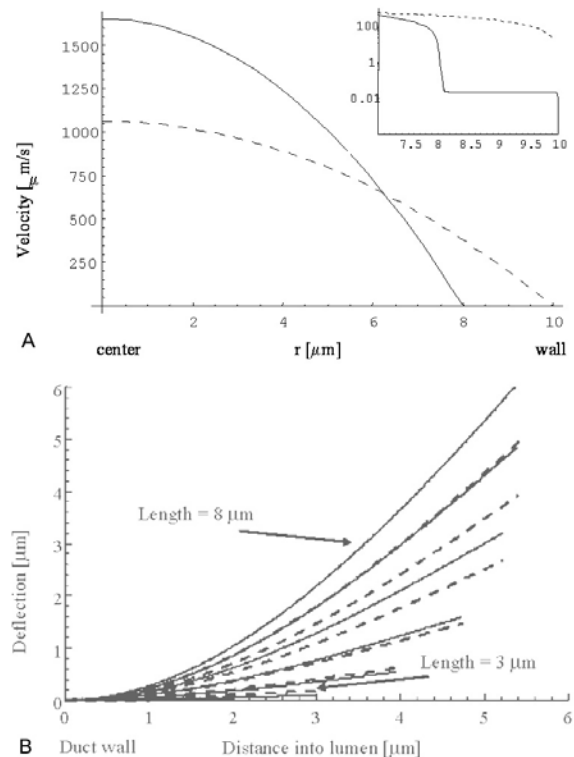


Figure 10. A. Comparison of the flow profile between unobstructed (dashed line) and obstructed (solid line) tubules. Calculations are based on constant volume flow of 10 nl/min, a tubule diameter of 20 μm , a brush border height of 2 μm , and a friction coefficient of 2800 $\text{cP}/\mu\text{m}^2$ (from Table 2, control flow). The inset is the region around the brush border, plotted on a logarithmic scale to better illustrate the flow. B. Deformation profiles of cilia in unobstructed (dashed line) and obstructed (solid line) tubules. Geometry and flow conditions are as in A, and flexural rigidity is taken as 31 $\text{pN}\cdot\mu\text{m}^2$. The cilium length is allowed to vary between 3 and 8 μm in length, i.e., 1 to 6 μm longer than the brush border when present. Note that short cilia bend less and long cilia more in the presence of a brush border compared to its absence. The switch from less bending to more occurs between cilium lengths of 4 and 5 μm .

For all of these effects, experiments are required to show functional links between (possible) mechanical stimulation of a cilium and unambiguous changes to cell function.

8. WHAT WILL BE THE DEFINING EXPERIMENTS?

Two typical biochemical manipulations of cilia are either inhibition of cilia growth or inhibition of ciliary-targeted proteins. In this manuscript, we have presented justification that in addition to these, experiments that act solely on mechanical deformations of cilia can yield

important information. To date, a few pioneering experiments have shown that fluid forces in tubules have definite consequences, for example Hove and Gharib's paper on cardiogenesis (78). This experiment clearly shows that mechanical forces determine ultimate differentiation states of developing organs. Future experiments that decouple mechanical and chemical effects will provide fundamental insights into mechanotransduction pathways as well. For example, observing *Clamydomonas* in a viscoelastic gradient would provide insight into how the cell responds to physical changes to the environment. Experiments that mechanically manipulate the cilium without fluid flow present would also be instructive.

9. CONCLUSION

Our hypothesis has been that the cilium mechanically transduces flow energy into stress energy, which is used to initiate flow-dependent signaling pathways. Some specific biological sequella of this hypothesis are that the ciliary length is regulated, that relevant proteins will be localized to the base of the cilium, and that the tubule diameter will be controlled. It has been shown experimentally that certain biochemical pathways are initiated in a flow-dependent manner, that PC1, PC2, STAT6 and P100 are localized at the base of the cilium, and that planar-cell-polarity-signaling pathways are ciliary dependent and control the growth of tubules. Thus, we already have evidence supporting our hypothesis, and we anticipate that the additional experiments outlined above will shed more information on this problem.

10. ACKNOWLEDGEMENT

This work was performed under the NIH HL41618, DK07678, DK27651, DK071027 and the Cystic Fibrosis Foundation R447-CR02 awards.

11. REFERENCES

1. Lamb, H. *Hydrodynamics*: Dover. (1945)
2. Resnick, A., Hopfer, U.: Force-response considerations in ciliary mechanosensation. *Biophys J* (in press) (2007)
3. Segel, L. A. *Mathematics Applied to Continuum Mechanics*. New York: Dover (1987)
4. Gottschalk, C. W., Mylle, M.: Micropuncture study of pressures in proximal tubules and peritubular capillaries of the rat kidney and their relation to ureteral and renal venous pressures. *Am J Physiol* 185: 430-439 (1956)
5. —: Micropuncture study of pressures in proximal and distal tubules and peritubular capillaries of the rat kidney during osmotic diuresis. *Am J Physiol* 189: 323-328 (1957)
6. Pruitt, M. E. C., Knepper, M. A., Graves, B., Schmidt-Nielsen, B.: Effect of peristaltic contractions of the renal pelvic wall on solute concentrations of the renal inner medulla in the hamster. *Am J Physiol -Renal Physiology* 290: F892-F896 (2006)
7. A. A. Kozinski, F. P. S., E.N. Lightfoot: Velocity Profiles in Pore-walled Ducts. *Ind Eng Chem Fundam* 9: 502-505 (1970)

Mechanical stimulation of primary cilia

8. Marshall, E. A., Trowbridge, E. A.: Flow of a Newtonian fluid through a permeable tube: the application to the proximal renal tubule. *Bull Math Biol* 36: 457-476 (1974)
9. Macey, R. I.: Pressure flow patterns in a cylinder with reabsorbing walls. *Bull Math Biol* 25: 1-9 (1963)
10. Middleman, S. Modeling Axisymmetric Flows: Dynamics of Films, Jets, and Drops: Academic Press.(1995)
11. Trowbridge, E. A. M. a. E. A.: Flow of a Newtonian Fluid Through a Permeable Tube: The Application to the Proximal Renal Tubule. *Bull Math Biol* 36: 457-476 (1974)
12. Han, Y. F., Ganatos, P., Weinbaum, S.: Transmission of steady and oscillatory fluid shear stress across epithelial and endothelial surface structures. *Phys Fluids* 17: - (2005)
13. Du, Z., Duan, Y., Yan, Q., Weinstein, A. M., Weinbaum, S., Wang, T.: Mechanosensory function of microvilli of the kidney proximal tubule. *Proc Natl Acad Sci USA* 101: 13068-13073 (2004)
14. Guo, P., Weinstein, A. M., Weinbaum, S.: A hydrodynamic mechanosensory hypothesis for brush border microvilli. *Am J Physiol* 279: F698-712 (2000)
15. Darcy, H. Les Fontaines Publiques de la Ville de Dijon. Paris: Dalmont. (1856)
16. Dillon, R. H., Fauci, L. J.: An integrative model of internal axoneme mechanics and external fluid dynamics in ciliary beating. *J Theor Biol* 207: 415-430 (2000)
17. A. A. Andronov, A. A. V., S. E. Khaikin. Theory of Oscillators. New York: Dover. (1987)
18. Sangani, A. S., Acrivos, A.: Slow Flow Past Periodic Arrays of Cylinders with Application to Heat-Transfer. *Int J of Multi Flow* 8: 193-206 (1982)
19. Sangani, A. S., Yao, C.: Transport Processes in Random Arrays of Cylinders .2. Viscous-Flow. *Phys Fluids* 31: 2435-2444 (1988)
20. Maunsbach, A. B., Giebisch, G. H., Stanton, B. A.: Effects of flow rate on proximal tubule ultrastructure. *Am J Physiol* 253: F582-587 (1987)
21. Knepper, M. A., Saidel, G. M., Hascall, V. C., Dwyer, T.: Concentration of solutes in the renal inner medulla: interstitial hyaluronan as a mechano-osmotic transducer. *Am J Physiol* 284: F433-446 (2003)
22. Nauli, S. M., et al.: Polycystins 1 and 2 mediate mechanosensation in the primary cilium of kidney cells. *Nat Genet* 33: 129-137 (2003)
23. Praetorius, H. A., Frokiaer, J., Nielsen, S., Spring, K. R.: Bending the primary cilium opens Ca²⁺-sensitive intermediate-conductance K⁺ channels in MDCK cells. *J Membr Biol* 191: 193-200 (2003)
24. Praetorius, H. A., Spring, K. R.: Bending the MDCK cell primary cilium increases intracellular calcium. *J Membr Biol* 184: 71-79 (2001)
25. —: Removal of the MDCK cell primary cilium abolishes flow sensing. *J Membr Biol* 191: 69-76 (2003)
26. Liu, W., Murcia, N. S., Duan, Y., Weinbaum, S., Yoder, B. K., Schwiebert, E., Satlin, L. M.: Mechanoregulation of intracellular Ca²⁺ concentration is attenuated in collecting duct of monociliium-impaired orpk mice. *Am J Physiol -Renal Physiology* 289: F978-F988 (2005)
27. Liu, W., Xu, S., Woda, C., Kim, P., Weinbaum, S., Satlin, L. M.: Effect of flow and stretch on the [Ca²⁺] response of principal and intercalated cells in cortical collecting duct. *Am J Physiol* 285: F998-F1012 (2003)
28. Preisig, P. A.: Luminal flow rate regulates proximal tubule H-HCO₃ transporters. *Am J Physiol* 262: F47-54 (1992)
29. Whitfield, J. F.: Primary cilium--is it an osteocyte's strain-sensing flowmeter? *J Cell Biochem* 89: 233-237 (2003)
30. Sanderson, M. J., Chow, I., Dirksen, E. R.: Intercellular Communication between Ciliated Cells in Culture. *Am J Physiol* 254: C63-C74 (1988)
31. Sanderson, M. J., Dirksen, E. R.: Mechanosensitivity of Cultured Ciliated Cells from the Mammalian Respiratory-Tract - Implications for the Regulation of Mucociliary Transport. *Proc Natl Acad Sci USA* 83: 7302-7306 (1986)
32. Ashkin, A., Dziedzic, J. M., Bjorkholm, J. E., Chu, S.: Observation of a Single-Beam Gradient Force Optical Trap for Dielectric Particles. *Opt Lett* 11: 288-290 (1986)
33. Ashkin A., D., J. M.: Observation of Resonances in the Radiation Pressure on Dielectric Spheres. *Phys Rev Lett* 38: 1351-1354 (1977)
34. —: Optical Levitation by Radiation Pressure. *Appl Phys Lett* 19: 283-285 (1971)
35. Lang, M. J., Block, S. M.: Resource Letter: LBOT-1: Laser-based optical tweezers. *Am J Phys* 71: 201-215 (2003)
36. Ashkin, A., Dziedzic, J. M.: Optical Trapping and Manipulation of Viruses and Bacteria. *Science* 235: 1517-1520 (1987)
37. Ashkin, A., Dziedzic, J. M., Yamane, T.: Optical Trapping and Manipulation of Single Cells Using Infrared-Laser Beams. *Nature* 330: 769-771 (1987)
38. Ashkin, A., Schutze, K., Dziedzic, J. M., Euteneuer, U., Schliwa, M.: Force Generation of Organelle Transport Measured In vivo by an Infrared-Laser Trap. *Nature* 348: 346-348 (1990)
39. Ghislain, L. P., Switz, N. A., Webb, W. W.: Measurement of Small Forces Using an Optical Trap. *Rev Sci Instrum* 65: 2762-2768 (1994)
40. Svoboda, K., Block, S. M.: Biological applications of optical forces. *Annu Rev Biophys Biomol Struct* 23: 247-285 (1994)
41. Svoboda, K., Schmidt, C. F., Branton, D., Block, S. M.: Conformation and elasticity of the isolated red blood cell membrane skeleton. *Biophys J* 63: 784-793 (1992)
42. Arya, M., Lopez, J. A., Romo, G. M., Dong, J. F., McIntire, L. V., Moake, J. L., Anvari, B.: Measurement of the binding forces between von Willebrand factor and variants of platelet glycoprotein Iba using optical tweezers. *Lasers in surgery and medicine* 30: 306-312 (2002)
43. Wright, W. H., Sonek, G. J., Berns, M. W.: Parametric Study of the Forces on Microspheres Held by Optical Tweezers. *Appl Opt* 33: 1735-1748 (1994)
44. Harada, Y., Asakura, T.: Radiation forces on a dielectric sphere in the Rayleigh scattering regime. *Opt Comm* 124: 529-541 (1996)
45. Gussgard, R., Lindmo, T., Brevik, I.: Calculation of the Trapping Force in a Strongly Focused Laser-Beam. *JOSA B-Optical Physics* 9: 1922-1930 (1992)
46. Barton, J. P., Alexander, D. R., Schaub, S. A.: Theoretical Determination of Net-Radiation Force and

Mechanical stimulation of primary cilia

- Torque for a Spherical-Particle Illuminated by a Focused Laser-Beam. *J Appl Phys* 66: 4594-4602 (1989)
47. Gouesbet, G., Lock, J. A.: Rigorous Justification of the Localized Approximation to the Beam-Shape Coefficients in Generalized Lorenz-Mie Theory .2. Off-Axis Beams. *JOSA A-Optics Image Science and Vision* 11: 2516-2525 (1994)
48. Lock, J. A.: Calculation of the radiation trapping force for laser tweezers by use of generalized Lorenz-Mie theory. I. Localized model description of an on-axis tightly focused laser beam with spherical aberration. *Appl Opt* 43: 2532-2544 (2004)
49. —: Calculation of the radiation trapping force for laser tweezers by use of generalized Lorenz-Mie theory. II. On-axis trapping force. *Appl Opt* 43: 2545-2554 (2004)
50. Lock, J. A., Gouesbet, G.: Rigorous Justification of the Localized Approximation to the Beam-Shape Coefficients in Generalized Lorenz-Mie Theory .1. On-Axis Beams. *JOSA A-Optics Image Science and Vision* 11: 2503-2515 (1994)
51. Neuman, K. C., Chadd, E. H., Liou, G. F., Bergman, K., Block, S. M.: Characterization of photodamage to escherichia coli in optical traps. *Biophys J* 77: 2856-2863 (1999)
52. Leitz, G., Fallman, E., Tuck, S., Axner, O.: Stress response in *Caenorhabditis elegans* caused by optical tweezers: Wavelength, power, and time dependence. *Biophys J* 82: 2224-2231 (2002)
53. Bartlett, P., Henderson, S.: Three-dimensional force calibration of a single-beam optical gradient trap. *J Phys-Condensed Matter* 14: 7757-7768 (2002)
54. Resnick, A.: Design and construction of a space-borne optical tweezer apparatus. *Rev Sci Instrum* 72: 4059-4065 (2001)
55. —: Use of optical tweezers for colloid science. *J Coll Interf Sci* 262: 55-59 (2003)
56. Low, S. H., Vasanth, S., Larson, C. H., Mukherjee, S., Sharma, N., Kinter, M. T., Kane, M. E., Obara, T., Weimbs, T.: Polycystin-1, STAT6, and P100 function in a pathway that transduces ciliary mechanosensation and is activated in polycystic kidney disease. *Dev Cell* 10: 57-69 (2006)
57. Adler, P. N.: Planar signaling and morphogenesis in *Drosophila*. *Dev Cell* 2: 525-535 (2002)
58. Baba, S. A.: Flexural rigidity and elastic constant of cilia. *J Exp Biol* 56: 459-467 (1972)
59. Deiner, M., Tamm, S. L., Tamm, S.: Mechanical properties of ciliary axonemes and membranes as shown by paddle cilia. *J Cell Sci* 104 (Pt 4): 1251-1262 (1993)
60. Schwartz, E. A., Leonard, M. L., Bizios, R., Bowser, S. S.: Analysis and modeling of the primary cilium bending response to fluid shear. *Am J Physiol* 272: F132-138 (1997)
61. Howard, J. *Mechanics of Motor Proteins and the Cytoskeleton*. Sunderland: Sinauer Associates, Inc. (2001)
62. Jurczyk, A., Gromley, A., Redick, S., San Agustin, J., Witman, G., Pazour, G. J., Peters, D. J., Doxsey, S.: Pericentrin forms a complex with intraflagellar transport proteins and polycystin-2 and is required for primary cilia assembly. *J Cell Biol* 166: 637-643 (2004)
63. Nauli, S. M., Rossetti, S., Kolb, R. J., Alenghat, F. J., Consugar, M. B., Harris, P. C., Ingber, D. E., Loghman-Adham, M., Zhou, J.: Loss of polycystin-1 in human cyst-lining epithelia leads to ciliary dysfunction. *J Am Soc Nephrol* 17: 1015-1025 (2006)
64. Kolb, R. J., Woost, P. G., Hopfer, U.: Membrane trafficking of angiotensin receptor type-1 and mechanochemical signal transduction in proximal tubule cells. *Hypertension* 44: 352-359 (2004)
65. Simons, M., et al.: Inversin, the gene product mutated in nephronophthisis type II, functions as a molecular switch between Wnt signaling pathways. *Nat Genet* 37: 537-543 (2005)
66. Andrade, Y. N., Fernandes, J., Vazquez, E., Fernandez-Fernandez, J. M., Arniges, M., Sanchez, T. M., Villalon, M., Valverde, M. A.: TRPV4 channel is involved in the coupling of fluid viscosity changes to epithelial ciliary activity. *J Cell Biol* 168: 869-874 (2005)
67. Michaud, E. J., Yoder, B. K.: The primary cilium in cell signaling and cancer. *Cancer Res* 66: 6463-6467 (2006)
68. Essig, M., Friedlander, G.: Tubular shear stress and phenotype of renal proximal tubular cells. *J Am Soc Nephrol* 14 Suppl 1: S33-35 (2003)
69. Kotsis, F., Nitschke, R., Boehlke, C., Bashkurov, M., Walz, G., Kuehn, E. W.: Ciliary calcium signaling is modulated by kidney injury molecule-1 (Kim1) *Pflugers Arch* 453: 819-829 (2007)
70. Lin, F., Hiesberger, T., Cordes, K., Sinclair, A. M., Goldstein, L. S., Somlo, S., Igarashi, P.: Kidney-specific inactivation of the KIF3A subunit of kinesin-II inhibits renal ciliogenesis and produces polycystic kidney disease. *Proc Natl Acad Sci USA* 100: 5286-5291 (2003)
71. Pazour, G. J.: Intraflagellar transport and cilia-dependent renal disease: the ciliary hypothesis of polycystic kidney disease. *J Am Soc Nephrol* 15: 2528-2536 (2004)
72. Jones, C., Chen, P.: Planar cell polarity signaling in vertebrates. *Bioessays* 29: 120-132 (2007)
73. Bisgrove, B. W., Yost, H. J.: The roles of cilia in developmental disorders and disease. *Development* 133: 4131-4143 (2006)
74. Singla, V., Reiter, J. F.: The primary cilium as the cell's antenna: signaling at a sensory organelle. *Science* 313: 629-633 (2006)
75. Banizs, B., Pike, M. M., Millican, C. L., Ferguson, W. B., Komlosi, P., Sheetz, J., Bell, P. D., Schwiebert, E. M., Yoder, B. K.: Dysfunctional cilia lead to altered ependyma and choroid plexus function, and result in the formation of hydrocephalus. *Development* 132: 5329-5339 (2005)
76. Snell, W. J., Pan, J., Wang, Q.: Cilia and flagella revealed: from flagellar assembly in *Chlamydomonas* to human obesity disorders. *Cell* 117: 693-697 (2004)
77. Li, J. B., et al.: Comparative genomics identifies a flagellar and basal body proteome that includes the BBS5 human disease gene. *Cell* 117: 541-552 (2004)
78. Hove, J. R., Koster, R. W., Forouhar, A. S., Acevedo-Bolton, G., Fraser, S. E., Gharib, M.: Intracardiac fluid forces are an essential epigenetic factor for embryonic cardiogenesis. *Nature* 421: 172-177 (2003)

Nomenclature (units in square brackets: L = length, T = time, M = mass), **Independent variables**, r: Radial coordinate, s: Deformed radial coordinate (section 5), t: Time, z: Axial coordinate, **Specified Functions**, $I_n(r)$: Modified Bessel Function of the first kind of order n, $K_n(r)$:

Mechanical stimulation of primary cilia

Modified Bessel Function of the second kind of order n ,
 $\ln(r)$: Natural logarithm, ∇ : Gradient operator ('nabla')
Dependent variables, Q_v : Volumetric flow rate [L^3/T], U :
Velocity [L/T], Parameters, A : Area of unit cell [L^2],
Vibration amplitude [L], a : Cilium radius [L], C_n :
Constants of integration, F_b : Body force density [M/L^2T^2],
 f : Force per unit length [M/T^2], g : Gravitational
acceleration [989 cm/s^2], K : Permeability coefficient [L^2],
 k : Coefficient of friction [M/L^3T], L : height of cilium [L],
 P : Pressure [M/LT^2], R : Lumen radius [L], Orbital shaker
throw distance [L], T : Stress tensor [M/LT^2], \mathcal{E} : Stress
energy per unit length [ML/T^2], α : decline constant [L^{-1}], δ :
height of brush border [L], ξ : area density of brush border
elements [L^{-2}], ρ : Density [M/L^3], μ : viscosity [M/LT], ω :
frequency [T^{-1}], **Dimensionless parameters**, Re : Reynolds
number, n : number of cylinders per unit cell, γ : Euler
constant, ϕ : Area fraction of brush border elements, χ :
Scaled area fraction of brush border elements

Key Words: Primary Cilium, Mechanosensation,
Mechanotransduction, Fluid Flow, Review

Send correspondence to: Dr Andrew Resnick, Department
of Physiology and Biophysics, Case Western Reserve
School of Medicine, 10900 Euclid Avenue, Cleveland OH
44106, Tel: 216-368-6899, Fax: 216-368-4223, E-mail:
Andy.resnick@case.edu

<http://www.bioscience.org/current/vol13.htm>